Taylor & Francis
Taylor & Francis Group

Engineering performance of tungsten network reinforced copper matrix composites synthesized by selective laser melting and infiltration

Fuxing Yao[a], Wenge Chen[a], Yana Yang[a], Kai Zhou[a], Rong Li[a], Ahmed Elmarakbi[b] and Richard Fu[b]

[a]School of Materials Science and Engineering, Xi'an University of Technology, Xi'an, Shaanxi, P.R. China;
[b]Faculty of Engineering and Environment, Northumbria University, Newcastle upon Tyne, UK

ABSTRACT

To solve poor engineering performance of copper-tungsten alloys operated at high temperatures, 3D network tungsten frameworks were prepared using a selective laser melting (SLM) process, and then copper was melted and diffused into these tungsten network structures to form copper matrix composites with different copper contents (i.e. Cu-10vol%W and Cu-30vol%W). Their mechanical/electrical properties and arc ablation performance were characterized. Results showed the obtained CuW composites were dense with good interfacial bonding, and the connected Cu phases formed a heat conduction channel and improved electrical and thermal conductivities of the composites. Electrical conductivities of Cu-30W and Cu-10W composites were 44.7% and 80.3% IACS, and their thermal conductivities at 25°C were 247.5 and 375.4 W/(m·K), respectively. The W-skeleton grid structure in the composites showed enhanced effects on impact toughness and anti-friction/wear resistance. Tensile strengths of Cu-30W and Cu-10W composites measured at 300°C were 95 MPa and 135 MPa, and their impact toughness values were 11.25 and 15.25 J/cm^2, respectively. For the arc ablation performance, the copper phase of CuW composite was identified as the key influencing phase, whereas the W skeleton effectively hindered the spread of arc spots, inhibited quick melting of copper phases, and played effective support and protection functions.
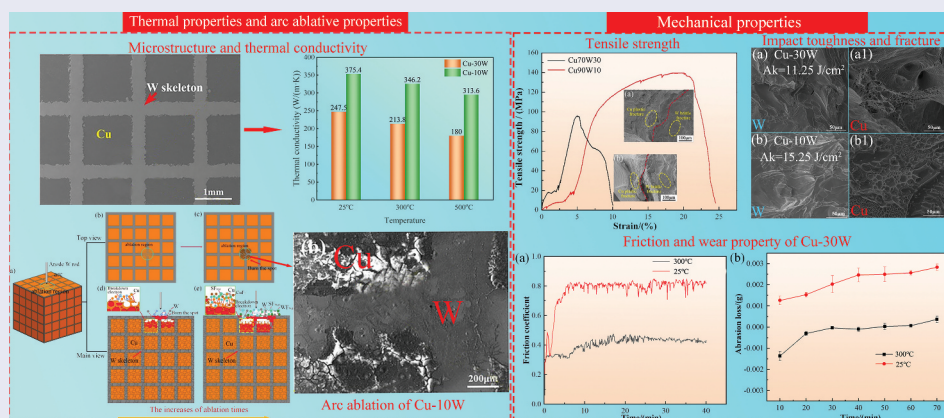
IMPACT STATEMENT

W network reinforced Cu matrix composites were prepared by combining 3D printing technology and fusion technology, which significantly improved the thermal and mechanical properties of Cu matrix composites. We find that the interconnected Cu phases improves the thermal properties of the composites, and the mesh W skeleton improves the mechanical properties.

1. Introduction

Copper and its alloys have excellent electrical and thermal conductivities, good ductility, machinability and corrosion resistance, and are widely used in various fields of electrical components, electronics, rail transit, packaging, machinery, energy/chemical industry, and aerospace [1]. For friction and wear performance in these fields, copper and copper alloys can no longer meet its application [2]. Copper matrix composite has been developed as an effective way to improve mechanical properties and functional properties of Cu materials. For example, ceramics with high hardness, high modulus and arc erosion resistance have been added into the copper matrix as the

strengthening phases to form copper matrix composites, which have excellent wear and corrosion resistance [3,4]. However, these ceramic particles are often susceptible to electron scattering, which reduces thermal and electrical properties of Cu-based composites [5]. The strength of copper matrix composites reinforced by precipitation phases [6–8] is usually decreased significantly at a high temperature, which cannot meet the stringent requirements for this application. When carbon nanotubes are used as the reinforcement material of copper matrix composites, strength, electrical and thermal conductivity of the composites can be significantly improved [9]. However, their wettability and interfacial compatibility between carbon nanotubes (CNTs) and Cu matrix are poor [10], often resulting in uneven dispersion of CNTs in the matrix and degrading the overall performance of CNTs/Cu matrix composites [11]. Bai et al. [12] prepared SiC/Cu composites using sol-gel and hot pressing sintering methods. Their microhardness was as high as 149.23 HV, the friction coefficient was as low as 0.34 ± 0.02, but their thermal conductivity was only 181.8 W/(m·K). Jiang et al. [13] prepared oriented SiC whisker reinforced Al_2O_3/Cu composites using powder metallurgy and hot extrusion processes, with an electrical conductivity of about 86.3% IACS.

Tungsten (W) has low coefficient of thermal expansion (4.5×10^{-6}/K), high hardness, good thermal stability [14], and good wettability with copper matrix, making it a good reinforcement material for copper matrix composites [15]. W reinforced Cu matrix composites usually have good electrical conductivity and mechanical properties, suitable for unique applications, such as heat sinks for highly loaded plasma facing components, and electrical contacts [16]. At present, preparation methods of CuW composites with high Cu contents mainly include vacuum sintering and spark plasma sintering (SPS) [17], vacuum sintering and hot extrusion [18]. However, microstructure distribution of CuW composites prepared by these processes is not easy to control, and their mechanical and thermal properties are still needed for improvement. In addition, tungsten skeleton with a high porosity (>50%) has been combined with infiltration sintering to obtain Cu-W composites with a high copper content (Cu content >50-vol.%), however, the formed composites often have the problem of low relative densities (<90%) [19].

Recently, the emerged metal additive manufacturing methodology provides a suitable tool for this purpose [20]. At present, this method has been applied to refractory metals and Cu matrix composites [21]. For example, Ambruş et al. [22] prepared copper-polylactic acid (PLA) filaments using fused deposition modeling technique, and studied their tensile properties. Dai et al. [23]

used selective laser sintering (SLM) technology to prepare WC/Cu composites and explored the influences of various process parameters on the densification of the composites. In addition, the SLM process was used to fabricate a tungsten skeleton with a porosity of more than 80% [24], showed a new route direction for preparation of CuW composites with high Cu contents. However, currently there are few studies on thermal and mechanical properties of CuW composites with high Cu contents using this SLM method.

In this study, porous tungsten frameworks with different porosities were prepared using the SLM method, and then copper billet was melted and diffused into this framework using a high temperature infiltration process. Using these processes, tungsten reinforced copper composites were successfully obtained with high strength, high density and high thermal conductivity. The influences of different porosities on mechanical properties and arc ablations characteristics of the composites were investigated and their microstructures and strengthening mechanisms were systematically studied.

2. Materials and methodology

2.1. Preparation of tungsten copper composites

In our previous study [25], porous tungsten framework was prepared and exhibited excellent performance when the porous structure was made into a square pattern. In this study, spherical tungsten powders with their particle sizes of 15–53 μm, provided by Institute of Materials and Processing of Guangdong Academy of Sciences, were used to prepare W skeleton with porosities of 70% and 90% using an EOS M290 selective laser melting equipment. The shapes and sizes of the designed W-skeleton are shown in Figure 1. Dimensions of W skeleton and CuW composite are $54.2 \times 10.9 \times 10.9$ mm³ (Cu-30W) and $55 \times 11.8 \times 11.8$ mm³ (Cu-10W), respectively. Pure copper powders with a purity of 99.9% and a particle size of 74 μm provided by Beijing Xingrongyuan Co., Ltd. were used as the raw material to be diffused into the porous W skeleton. Cu-30W and Cu-10W composites (with 70% and 90% Cu in volume percentages) were prepared using a fusion sintering technology.

Figure 1 shows the preparation processes for the nanocomposite. Tungsten skeleton was prepared using the SLM process, and the process parameters are listed in Table 1. Afterwards the HF and HNO_3 were used to clean the surfaces of the printed skeletons. All the samples were heated to 1300°C in an argon atmosphere. The copper billets were melted for 90 min and diffused into the skeletons of W under the atmospheric pressure. The network tungsten reinforced copper matrix composites were obtained after cooling down to room temperature.
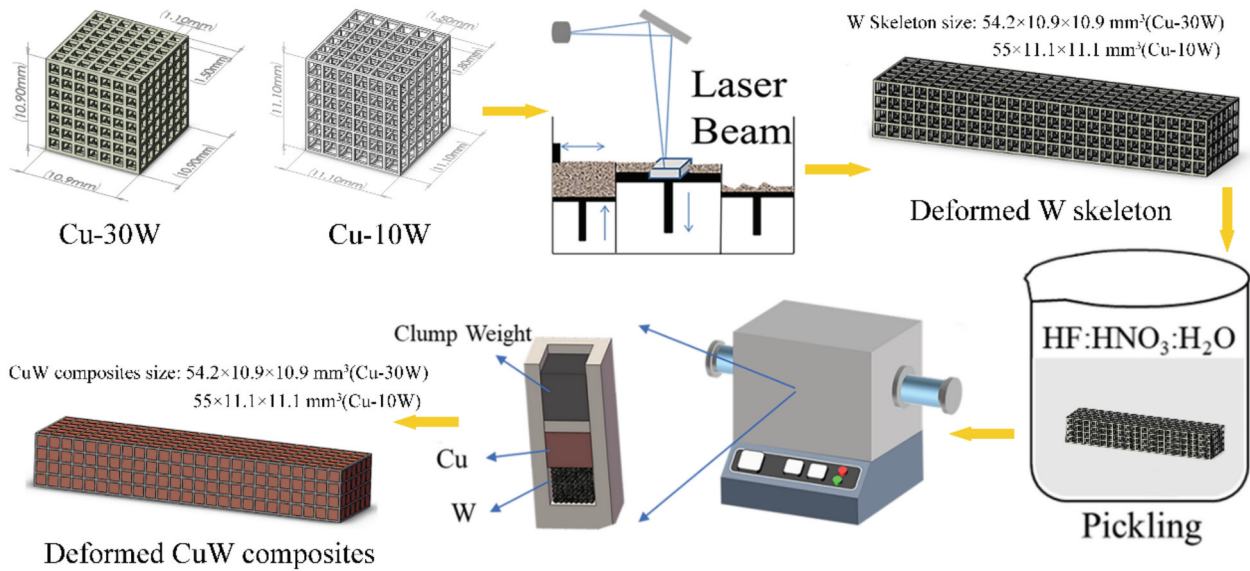
Figure 1. Illustrations of fabrication process of tungsten network reinforced copper matrix composites.

Table 1. Main parameters of laser selective melting printing skeleton.

Major parameters	Values
Powder-bed depth	25 μm
Spot diameter	100 μm
Laser power	120W
Scan speed	550 mm/s
Scan interval	60 μm
Inert gas flow	1~3 m^3/h

2.2. Characterization methods

Crystalline structures of Cu-W nanocomposites were analyzed using an X-ray diffractometer (XRD, XRD-7000S, Japan) with Cu-Kα radiation, under a scanning speed of 8 deg/min. Its morphology was observed using a field emission scanning electron microscope (FE-SEM, JEOL JSM-6700F, Japan), and the chemical elements at the interfaces of the Cu-W composite were characterized using an energy dispersive X-ray spectrometer (EDS). Electrical conductivity of the composites was characterized using a digital conductivity meter (D60K, DSS Electronics, China). Its density was measured using an Archimedes method with an electronic analytical balance (ESJ200-4, LONGTEBF Electronic, China, with a resolution precision of 0.1 mg), and the relative density was calculated using Equation (1). Its high temperature mechanical properties were tested at 300°C using a tensile testing machine (CMT5105, MTS, China) according to Chinese Standard T228.1-2010, China. The tensile specimens had a dimension of $23 \times 6 \times 2$ mm^3, and the tensile strength fof the composite was calculated using Equation (2).

$$\rho = \frac{\rho_0}{\rho_{CuW}} \quad (1)$$

$$\sigma_b = F_b / S_0 \quad (2)$$

where ρ_{CuW} is the theoretical density of CuW composites, ρ_0 and ρ are the actual measured density and relative density of Cu-W composite, σ_b is the tensile strength. F_b is the maximum force of the specimen when it is broken. S_0 is the original cross-sectional area of the sample. A laser flash thermal conductivity tester (LFA 427, NETZSCH, Germany) was used to measure the thermal conductivity at testing temperatures of 25°C, 300°C, and 500°C. The standard size of thermal conductivity testing sample was $\Phi 12.7$ mm $\times 1.5$ mm, and the heat capacity of the composite was obtained by comparing with that of the graphite's standard pattern. According to Chinese Standard T229-2020, the Charpy impact toughness of Cu-30W composites was tested at 25°C using a JB-30 impact testing machine. Charpy V-notched impact samples ($55 \times 10 \times 10$ mm^3) were used for the impact tests. The HT-1000 high-temperature friction and wear testing machine was used to carry out dry friction and wear tests at room temperature and 300°C. The sample size was $4 \times 4 \times 10$ mm^3, and the counter face material was HT250 gray cast iron disc with a diameter of 30 mm and a hardness of 209 HB. Before the test, the surface of the sample and friction pair were cleaned with alcohol to remove any particles and impurities. During the testing, the load was set at 15 N and the speed was set at 500 r/min. The samples were taken down every 10 minutes, and the weight of the worn samples was weighed on an electronic balance with an accuracy of 0.1 mg to calculate the mass loss of the samples over time. The microstructure of CuW composites after friction and wear was analyzed using SEM and EDS.

Arc ablation experiments of the composites were carried out in SF$_6$ arc extinguishing atmosphere using
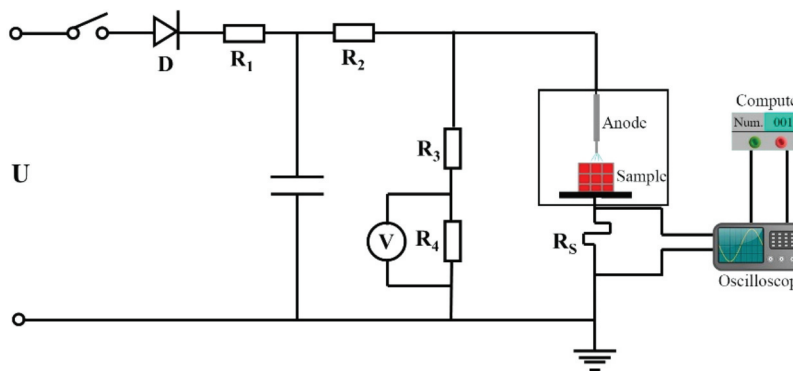
Figure 2. Schematic diagram of arc ablation experimental device.

a home-made high voltage breakdown tester (as illustrated in Figure 2). Samples size of the Cu-W composite cube for the arc ablation experiments was $10 \times 10 \times 10$ mm^3. The anode of arc ablation tester was a tungsten rod with a diameter of 5 mm and a tip diameter of 0.5 mm. During the experiments, the cathode was moved slowly to the anode. At a DC voltage of 10 kV, an arc was generated between two electrodes, and the first arc breakdown process was conducted.

3. Results and discussion

3.1 Microstructure and morphology of composites

Figure 3 shows an SEM image of Cu-30W composite (here the numbers of 70 and 30 indicate volume percentage ratios of Cu and W), in which copper is melted and diffused into the tungsten skeleton with a square shape. There are no apparent defects or pores in the gray-black copper phase along both vertical (Figure 3(a)) and parallel directions of the laser process direction (Figure 3(b)). It can be seen from Figure 3(a1,b1) that there are a small number of microcracks in the W skeleton, which are formed under the actions of thermal stress and residual stress caused by the slow movement of laser beam during the preparation of W skeleton. However, after the infiltration with Cu, these microcracks are filled with copper to form a relatively dense composite. EDS analysis of the interface shows that the width of the interface transition layer is less than 0.5 μm (see Figure 3(a2)), revealing a quite 'smooth' bonding interface [26]. This structure helps to improve the bonding strength between the insoluble W and Cu.

Figure 4 shows the SEM images of Cu-10W composites prepared with a square shaped tungsten framework. As can be seen from images, the molten copper phase within the skeleton phase is clearly observed in both the vertical and parallel processing directions. The black areas were identified as the copper phase, and gray ones were identified as the pure tungsten
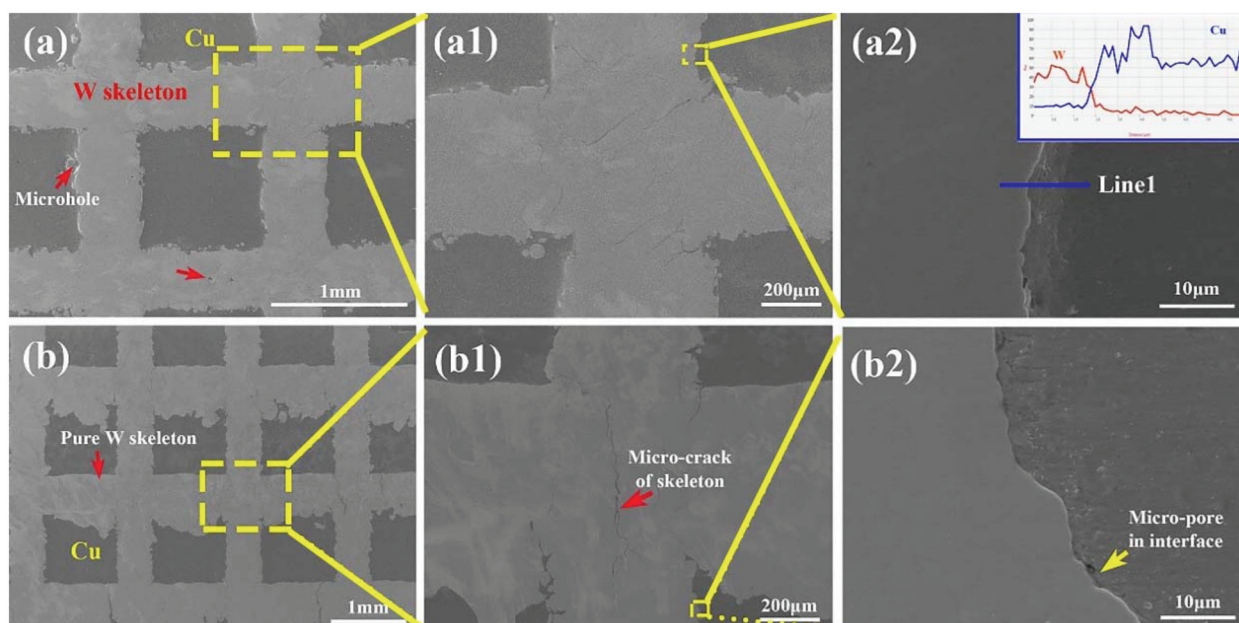
Figure 3. SEM image of Cu-30W composite prepared by Cu-phase square melting in tungsten framework; (a–a2) Vertical printing direction; (b–b2) Parallel to the printing direction.
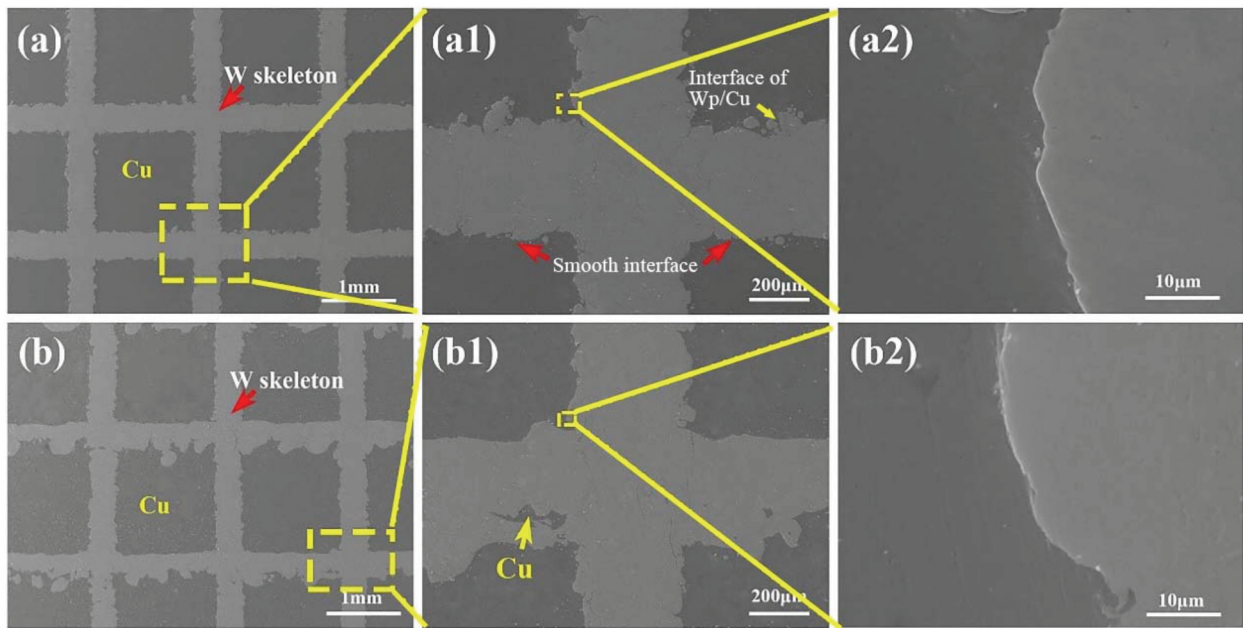
Figure 4. SEM image of Cu-10W composite prepared by Cu-phase square melting in tungsten framework; (a–a2) Vertical printing direction; (b–b2) Parallel to the printing direction.

skeleton phase. The enlarged interface image in Figure 4 shows that there is no micropore or gap, indicating that the copper phase has been filled into the spaces of network tungsten skeleton during the melting and infiltration processes. Compared with those of Cu-30W composites, the W skeleton defects are significantly reduced, indicating better mechanical properties.

Figure 5 shows the XRD patterns of CuW composites with different Cu/W contents. Comparing the diffraction peaks in the figure with the standard PDF cards of pure copper (PDF#85-1326) and pure tungsten (PDF#04-0806), it was found that the diffraction peaks are mainly W and Cu ones without other diffraction peaks. This indicates that there is no oxidation or formation of other substances during the preparation of tungsten copper gradient composite materials. The higher the Cu content, the stronger the diffraction peak of Cu. Analysis of the XRD patterns using the Rietveld method shows that the content of W in Cu-30W composite is 32.3 Vol %, and that of Cu is 67.7 vol%. Whereas, the content of W in Cu-10W composite is 10.9 vol %, and that of Cu is 89.1 vol %.
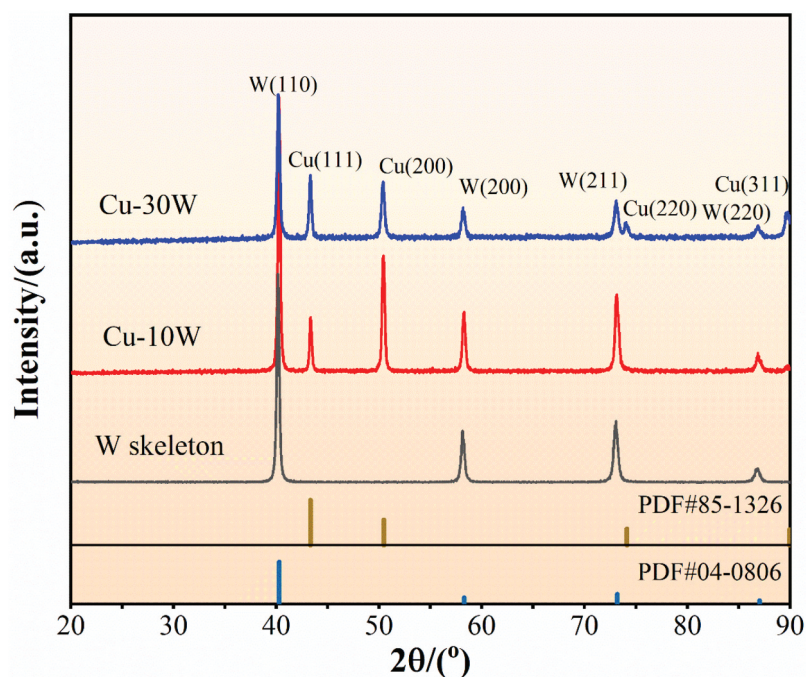
Figure 5. XRD patterns of network-like tungsten reinforced copper matrix composites.

3.2. Physical and mechanical properties of composites

Table 2 lists the obtained properties of CuW composites. Clearly the higher the content of W is, the higher the density of composite is, which is mainly because the density of W is much higher than that of Cu. The lower relative density of Cu-10W composite may be due to the influences of copper capillary force and grain boundary diffusion during the copper infiltration. The porosity of W skeleton in the Cu-10W composite is significantly higher than that in the Cu-30W composite, even though the sintering time of Cu-10W composite is the same during copper infiltration. Due to the influence of the gas in the pores, the molten copper phase cannot be fully filled into the W skeleton, which reduces the density of the composite material.

As listed in Table 2, the conductivity and thermal conductivity of the Cu-30W composites are almost half of those for the Cu-10W composites. This is mainly because the Cu content has great effects on the conductivity and thermal conductivity of composites. With the same network shape, the less tungsten content is, the higher the electrical conductivity is. This is easily understood as the electrical conductivity of copper is significantly larger than that of the tungsten [27]. The tungsten network reinforced copper matrix composites in this study show much higher conductivity values than those of the fiber tungsten reinforced copper matrix composites reported in Ref [28]. Compared with the CuW composite powder prepared using the co-precipitation method by Wang et al. [17], the conductivity of Cu-10vol %W composite prepared using the powder sintering method in this study has been significantly improved, and the conductivity is similar to that of Cu-20 wt%W prepared using the spark plasma sintering method by Li et al. [14] In this network-based composite, tungsten and copper phases are interconnected, and the copper phases are effectively infiltrated inside the skeleton structures. This helps to reduce the scattering of free electrons, thus leading to an increase in conductivity [29]. On the other hand, the decrease of porosity and

increase of W content result in the increase of the width of W skeleton, which weakens the channeling effect of Cu in the composite, thus affecting the conductivity of materials. The thermal conductivity values of all the composites decrease with the temperature, mainly because the increased thermal resistance (due to the increase lattice vibrations and impurity defects at a higher temperature) will hinder the movement of free electrons [30]. When the testing temperature is the same, the higher the copper content of the composite is, the higher the thermal conductivity. Compared with the result reported in Ref. [31], the differences in thermal conductivity values of the different composite are mainly influenced by the shapes of network structures and distribution of copper inside this tungsten skeleton. The square shaped network structure with a copper content of 90% has the highest thermal conductivity of 375.4 W/(m·K) at 25°C. At 500°C, the thermal conductivity of the square shaped network structure with a copper content of 90% can still be maintained at 313.6 W/(m·K). This value is similar to the thermal conductivity of Cu/diamond composite (377 W/(m·K)) [32] and CuAg alloy (375.48 W/(m·K)) at 550°C and 600 MPa [33].

As can be seen from Figure 6, compared with the composites of similar compositions [14,15,17,34–36], the CuW composites prepared in this study show a similar microhardness, but a higher conductivity, which is mainly related to the connected structures of the Cu phase in this composite. However, the Cu-30W composites show a slightly lower conductivity, which is mainly because the increase in the content of W reduces the conductivity of the CuW composites.

As the composites are mainly used for high temperature applications, the tensile stress-strain curves of the composites tested at a high temperature of 300°C were obtained and the result are shown in Figure 7. The curves show the different stages of elastic deformation, plastic deformation, and fracture, without an apparent yielding stage. The slope of Cu-30W composite at the elastic stage is larger than that of Cu-10W, indicating that the elastic modulus of Cu-30W composite is higher than that of Cu-10W composite. This is because the elastic modulus of W (411 GPa) is much larger than that of copper (117 GPa), and the higher the content of W is, the larger the elastic modulus of the composite. The maximum strengths of Cu-30W and Cu-10W are 95 MPa and 135 MPa. If compared with that of pure copper [24], the increase in the strength is 90% and 170%, respectively, and their elongation rate are ~ 5% and ~ 20%, respectively.

Interestingly, the tensile strength and elongation of the Cu-30W composite are lower than those of the Cu-10W composite. This is because the higher the content of W in the porous tungsten is, the longer distance of the mesh lines is, thus the more overlapping ration in the laser printing. In the laser beam process, the heat

Table 2. Comparison of density and relative density parameters of network-skeleton reinforced copper composites with different specifications.

Sample		Cu-30W	Cu-10W
Theoretical density(g/cm^3)		12.244	10.415
Density(g/cm^3)		12.084 ± 0.075	10.184 ± 0.067
Relative density		98.69%	97.78%
Conductivity(%IACS)		44.7 ± 0.86	80.3 ± 0.73
Vickers hardness (HV)		113.23 ± 1.42	156.4 ± 1.13
Thermal diffusivity	25°C	77.52 ± 0.25	109.57 ± 0.32
	300°C	66.96 ± 0.45	101.05 ± 0.39
	500°C	56.37 ± 0.47	91.53 ± 0.38
Thermal conductivity	25°C	247.5±0.98	375.4±1.35
(W/m·K)	300°C	213.8 ± 1.76	346.2 ± 1.67
	500°C	180.0 ± 1.83	313.6 ± 1.59
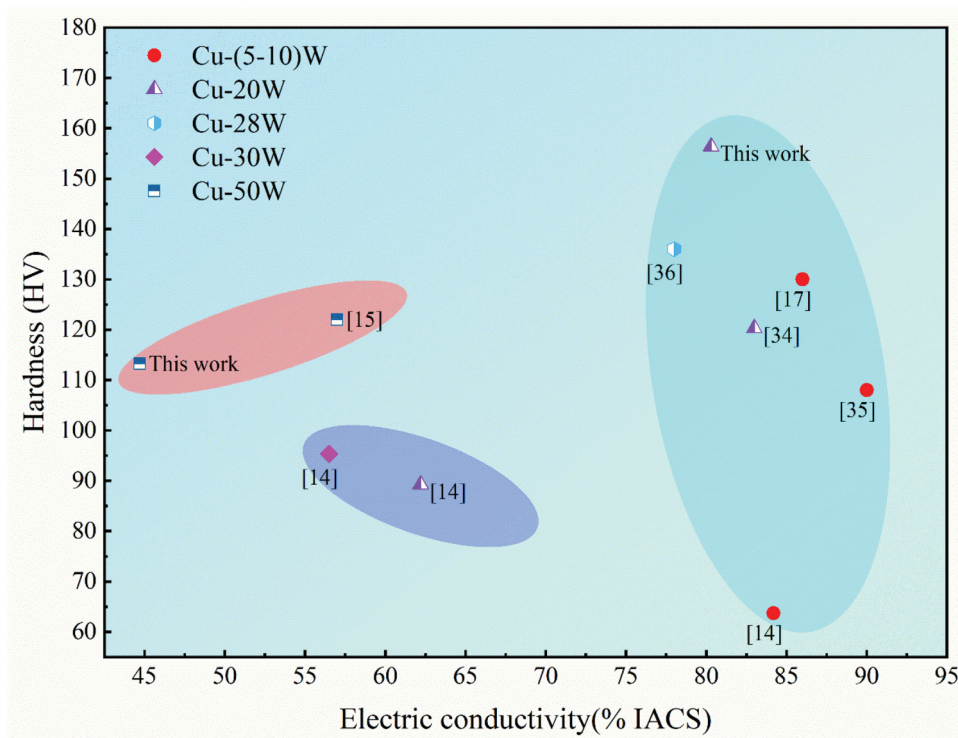
Figure 6. Comparison of properties of CuW composites with high Cu content [14,15,17,34–36].

dissipation is not quick enough, thus resulting in the accumulation of a large amount of thermal stress between adjacent layers and formation of more defects during cooling. At a high temperature, these cracks become weak positions in the composite material. Under a large tensile stress, the cracks are propagating until fracture of the composite, thus reducing the ultimate tensile strength of the material. The sudden drop in tensile stress in the curve is caused by the sudden breaking of the W skeleton. Smooth neck

platform shown in the curve indicates a typical ductile fracture behavior of porous metallic materials [37]. On the other hand, Cu and W contents also affect the mechanical properties of materials [38]. The defects of Cu-10W composite are significantly reduced, and the Cu-10W composite exhibits good strengthening effect under tensile stress, and there is no obvious necking step at the fracture stage.

The insets in Figure 7 shows the fracture morphologies of square shaped skeletons composites. Fracture
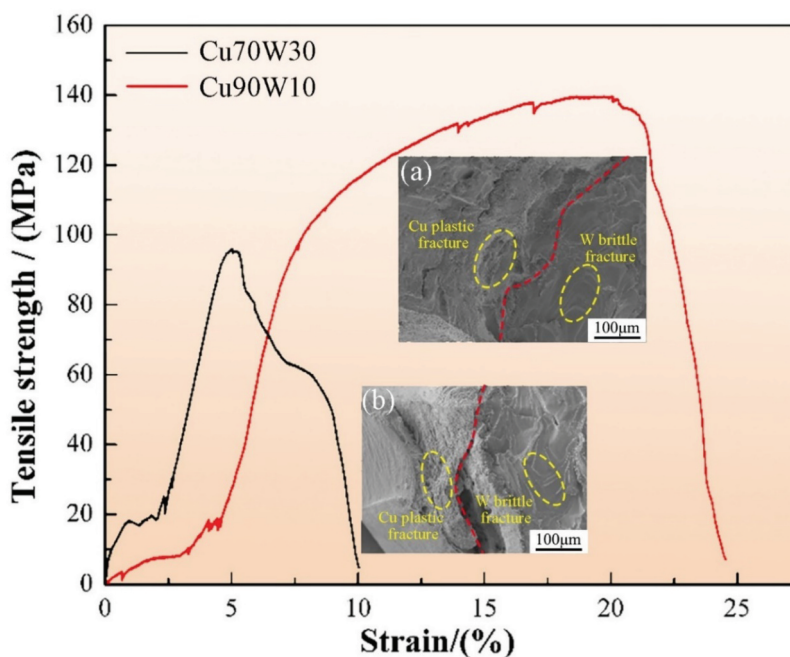
Figure 7. Stress-strain curves of network-shaped tungsten reinforced copper matrix composites at 300°C.

mostly occurs at the boundaries between skeletons and pure copper phases. The gaps between skeleton phase and copper phase become much larger after stretching. Figure 7(a,b) show the tensile fracture morphologies of Cu-10W and Cu-30W composites, respectively. It can be seen from these figures that the tensile fracture morphology of Cu-10W composite presents folded features, linking to its ductile fracture. In contrast, the fracture surface of Cu-30W composite is relatively smooth and flat, which is corresponding to the cleavage fracture feature. Micro-size cracks are found at the Cu and W interfaces.

The main reasons for the brittle fracture and low strength values of the composites can be summarized as follows. Firstly, the 3D laser printing leads to the anisotropic features of the tungsten skeleton, which makes the mechanical properties of the skeleton much different in different directions [39]. Secondly, the laser printed tungsten skeleton structures have many microscale pores, which prevent copper to be effectively infiltrated inside network structures (see in Figure 3(b2)). Thirdly, there is minimized solubility between tungsten and copper, and only atomic diffusion can happen at their interfaces. This results in a poor bonding strength between them.

The obtained impact toughness of Cu-30W and Cu-10W composites are 11.25 J/cm^2 and 15.25 J/cm^2. Compared with that of copper (19.6 J/cm^2 [40]), the impact toughness values of the composite are decreased, but the obtained impact toughness is still much higher than that of ordinary Cu alloy (e.g. for CuCrNi alloy, this value is 0.83 J/cm^2 [41]). In addition, the rigid W skeleton of CuW composites was used as a reinforcing phase to improve the strength of the material in this study, and the ductile Cu phase is the main component to resist the plastic deformation. Therefore, Cu-10W composites with a higher Cu content show a higher impact toughness. In the process of impact fracture, cracks are firstly formed at the interfaces, and then continuously propagated until the fracture of the composite, thus reducing the overall impact toughness of the material. On the other hand, compared with that of the brittle tungsten, copper with a much better plasticity is effective in absorbing fracture energy.

Figure 8 shows SEM images of impact fracture morphology of Cu-30W and Cu-10W composites. The interfacial feature is shown in Figure 8(a). The crystalline tungsten skeleton (shown in the blue dashed line frame) and the fibrous copper phase (shown in the red dashed line frame) are evenly distributed. There is obvious separation of W and Cu phases at the interface, thus forming a brittle and gully morphology. This is mainly caused by the poor wettability of W and Cu phases and poor interfacial bonding. At a higher magnification, the skeleton shape of tungsten presents cleavage steps (see Figure 8(b)),

which are a typical cleavage brittle fracture morphology. In the copper phase, many dimples and fibrous morphologies of different sizes can be observed (see Figure 8(c)), which is similar to the tensile fracture morphologies shown in Figure 6, indicating a typical ductile fracture.

Figure 8(d–f) show the impact fracture morphology of Cu-10W composite. Compared with Cu-30W composite, Cu-10W composite has the same fracture mode and similar fracture morphology at the interfaces and W skeleton. However, there is more severe plastic deformation in the Cu phase. This is because the higher the Cu content is, the better the plastic deformation ability of the composite material, which is also an important reason for the high impact toughness of Cu-10W composite material.

The friction coefficient and wear resistance of Cu-30W and Cu-10W composites were evaluated in order to explore the effect of W skeleton on the wear resistance of W reinforced Cu matrix composites. Figure 9(a) shows the friction coefficient of Cu-30W and Cu-10W composites tested at 25°C and 300°C. As can be seen from the figure, at room temperature, the friction coefficient of CuW composite material increases sharply at the beginning, but then gradually becomes stable. This is because at the beginning of wear process, the contact between the friction pair and the sample is mainly point contact with small contact area and a low friction coefficient. The contact area is increased with the increase of testing time, resulting in the increase of friction coefficient [42]. The friction coefficient changes a little with the increase of contact areas and eventually becomes stable. However, the friction coefficient of composite material becomes totally different at 300°C, which is mainly because the composite material presents a good plasticity at high temperature with the decreased hardness. The friction coefficient of the composite at a high temperature of 300°C (~0.45) is much lower than that at room temperature (~0.8). This is because copper and tungsten are easily oxidized at a high temperature. The high melting point and high hardness of the oxides provide a transient protective layer for the CuW composites, which results in the low friction coefficient of CuW composites tested at a high temperature [42]. As is well-known, the oxidation kinetics of materials depends significantly on oxygen concentration and temperature [43]. The oxidation of CuW composites in this study is also strongly dependent on temperature. Even though the temperature of 300°C is not high enough to significantly oxidize the material, the copper matrix composite tends to be oxidized and softened [44]. Combined with Figs. 12(b2,c2), we can conclude that the O content of the composite material after friction and wear at high temperature is significantly increased (about
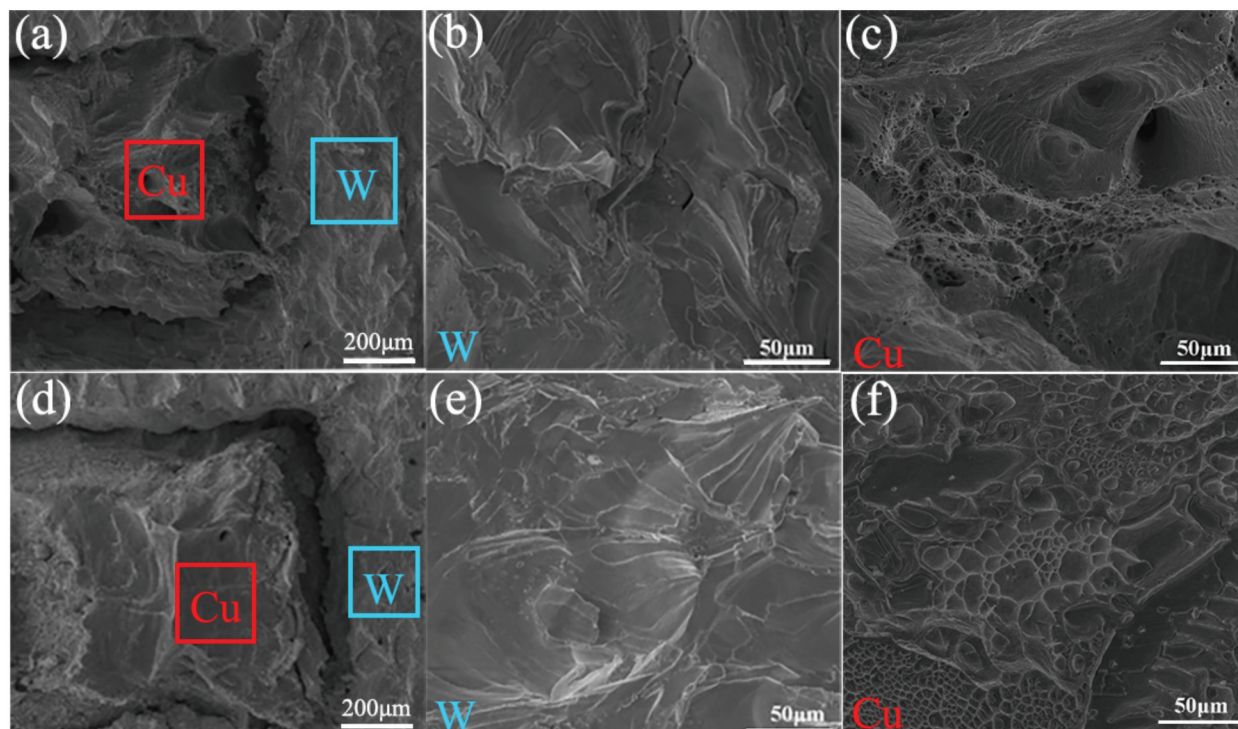
Figure 8. SEM image of impact fracture of Cu-30W and Cu-10W composites. (a ~ c) Cu-30W; (a) Interface morphology, (b) Tungsten phase; (c) Copper phase; (d ~ f) Cu-10W; (d) Interface morphology, (e) Tungsten phase; (f) Copper phase.

twice that of friction and wear at 25°C), which indicates clearly that the oxidation degree of Cu and W phases is intensified at the high temperature. The formation of oxides improves the surface hardness of the composite material and provides a transient protective layer for the composite material. The W skeleton distributed in the network also mitigate the severe wear of CuW composites, which also results in the low friction coefficient of CuW composites tested at high temperatures.

Figure 9(b) shows the wear losses of composite materials tested at 25°C and 300°C. It can be seen from the figure that the wear losses of composite materials measured at room temperature and high temperature firstly increase with the increase of time, and then gradually becomes stable. This is because at the initial stage of friction and wear, the micro-asperities on the surface firstly contact with the friction pair, causing the spallation and the quite wear of these micro-asperities. With the increase of the contact area, the wear process becomes stable and the wear volume gradually becomes stable. Interestingly, at the initial stage of friction and wear at 300°C, the wear amount of the composite material is negative, and the curve shows a weight increase. After 50 min, the wear amount of the composite material changes to positive, and the mass of the composite material begins to decrease. This is because copper and tungsten will be oxidized to form oxides at high temperature, and the mass of composite material is increased when they are oxidized. At the beginning of friction

and wear, the wear amount of composite material is less than the mass increased by the oxidation of composite material surface, so the wear amount of composite material is negative. In addition, the highly hard tungsten oxide forms a good protective layer on the surface of the composite material, preventing the quick wear of the material. With the increase of wear duration, the worn area is gradually increased, and then the wear becomes stable. The wear amount is greater than the oxide production amount, which shows that the wear amount is positive and stable, and the mass of the composite decreases.

As can be seen from Figure 9(a,c), at the same Cu content, the friction coefficient at the high temperature is significantly lower than that at room temperature. Due to the softening of copper at high temperature, a self-lubricating layer could be formed on the surface of the composite material, thus reducing the friction coefficient of the composite material. With the increase of Cu content, the friction coefficient of Cu-W composite increases significantly at room temperature, mainly because the increase of copper content reduces the hardness of the composite, and the Cu phase is easily sticked to the friction pair, thus increasing the friction coefficient of the material. However, the friction coefficient of Cu-30W composite is significantly higher than that of Cu-10W. This is mainly related to the 'stick-slip' phenomenon in composite materials, in which stiction or adhesion and sliding occur alternately [45]. In addition, the friction process will also produce certain abrasive chips, the
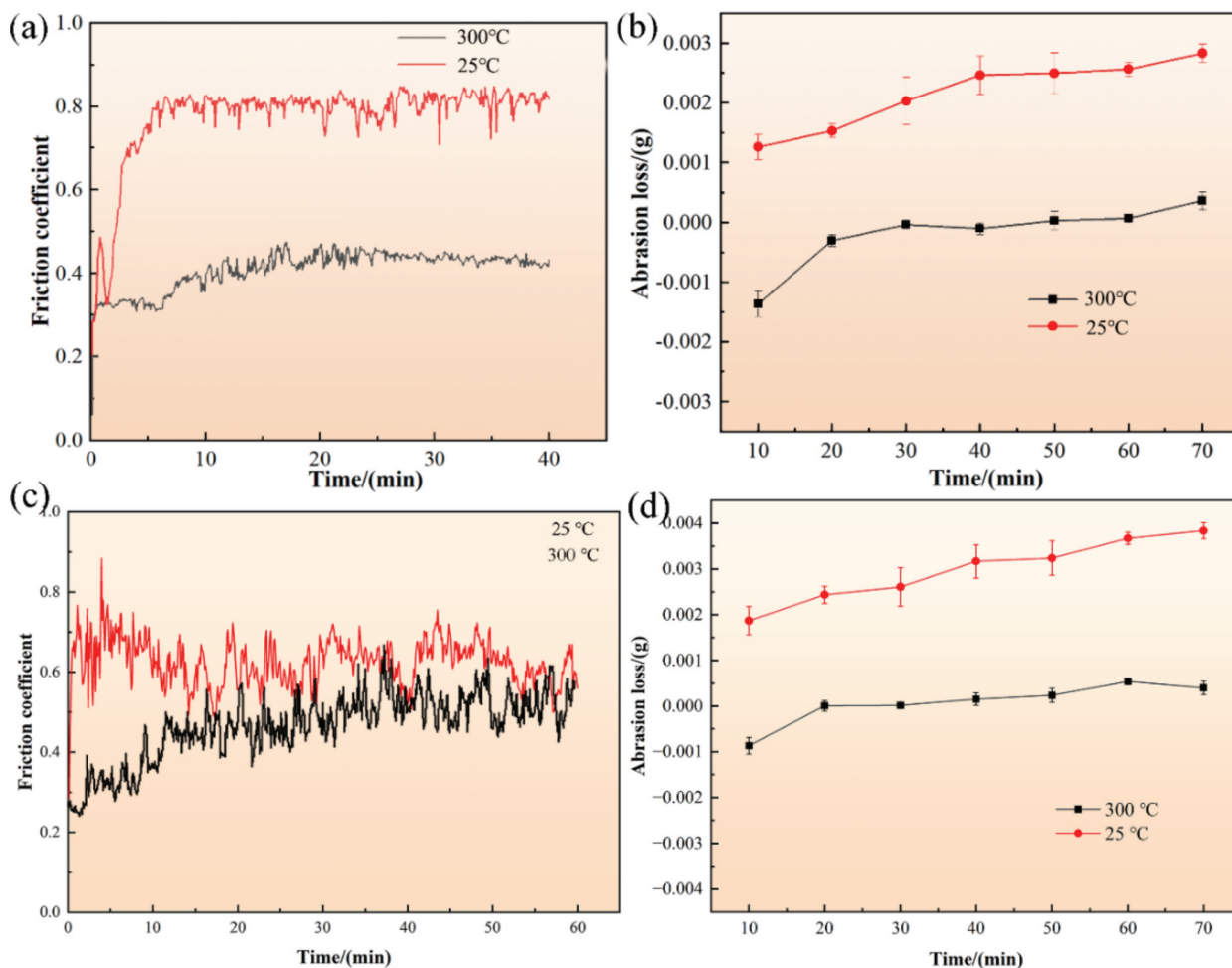
Figure 9. (a) Friction coefficient of Cu-30W composites at different temperatures; (b) Wear capacity of Cu-30W composites at different temperatures.

outcome of which will reduce the contact area and act as the lubricant. However, abrasive chips will lead to serious abrasive wear, resulting in large fluctuations in the friction coefficient [46]. It can be seen from Figure 9(b,d) that although the trend of ablative mass loss of the composite is the same, the wear mass loss of the Cu-10W composite is significantly larger than that of the Cu-30W composite. This is mainly attributed to the easy shedding of the Cu phase with lower hardness during the friction and wear process.

Figure 10 shows the worn morphology of the composite material at 25°C. From Figure 9(a,a1), it can be observed that two different friction-wear morphologies appear at the interface of the composite material. The W phase shows obvious furrow morphology, and there are many particles in the Cu phase. At a higher magnification, there are many furrows shaped wear marks on the worn surface of W skeleton region A, and white particles are also observed on the wear marks (see Figure 10(b,b1)). The EDS spectrum of particles is shown in Figure 10 (c2) and can be divided into W and O components. These particles are mainly formed by the brittle fracture of the incompletely melted W particles in the

wear process. The brittle and broken particles cut the composite materials under the action of shear stress, forming furrow patterns. This clearly indicates that the wear mode of the W skeleton region is mainly abrasive wear. It is observed from Figure 10(c,c1) that there are many granular spots in copper phase at region B, which is related to the wear debris formed after wear. EDS analysis of these particles (see Figure 10(c2)) shows that the particles contain Fe, O and Cu. This indicates that after a long time of wear, there are a lot of heat generated at the friction surface, so that the Cu phase and the surface of the friction pair are quickly oxidized to form an oxide layer, which is adhered to the surface of the composite material. There are both adhesive wear and oxidation wear in the Cu phase zone, and the Cu phase zone is covered with wear marks. In addition, wear debris will further slide between the gaps in pits and grooves on the surface of the filling material, making the surface relatively smooth, thus reducing the wear rate of the composite material [42].

Figure 11 shows the surface morphology of Cu-30W composites worn at 300°C. As shown in Figure 11(a,a1), it is found that the flake chips and
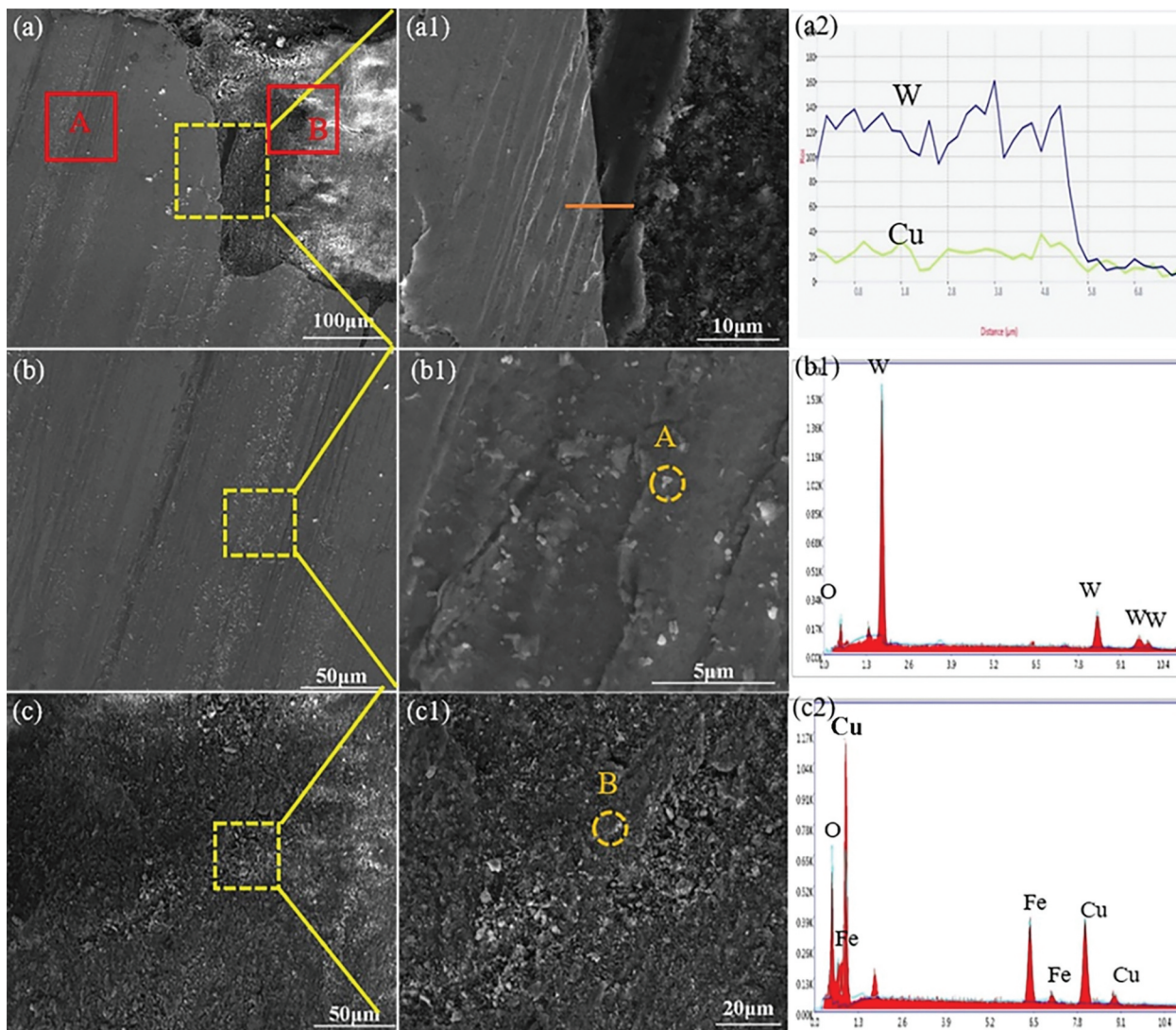
Figure 10. Surface morphologies of copper tungsten composites worn at room temperature (a–a2) Morphology and EDS spectrum of composite after wear; (b–b1) The enlarged part of region a in figure (a) and its EDS spectrum; (c–c1) Enlarged portion of region B in figure (a) and its EDS spectrum.

several particles can be observed on the worn surface of the composite material at high temperature. Compared with the friction and wear morphology at room temperature, no obvious furrow morphology is appeared on the surface. Enlarged region A in Figure 11(a) shows that there are a lot of chips observed on the surface of the material (see Figure 11(b,b1)). EDS analysis was performed on the chip grindings (see Figure 11(b2)) and it was found that the main components of the grindings were W, Fe and O. It indicates that the surface of the friction pair is oxidized and removed in the process of friction and wear at high temperature. The lamellar wear chips are generated on the composite surface after a long-term wear. The friction and wear coefficient of the composite are significantly reduced, and show a protective effect on the surface of the composite. The enlarged images in region B of Figure 11(a) shows that many particles are existed on the surface of the composite material (see Figure 11(c,c1)), and the composition

elements of these particles are Cu, O and Fe. It clearly shows that the oxide layer is formed by oxidation of Cu surface and friction pair at a high temperature. In the process of friction and wear, the oxides formed on the surfaces of the friction pair fall off and then are sticked to the surface of the composite material. The debris falling off the surface of the friction pair constantly destroys the oxide layer on the surface of the composite material, making the oxide layer become particles of different sizes attached to the surface of the composite material. Numerous particles are accumulated on the surface of CuW composites after a long time of wear, which indicates that the wear mechanism of CuW composites at 300°C is the combination of abrasive wear, adhesive wear, and oxidation wear. In the process of friction and wear, the worn surface of the composite material is flat, and the high hardness W skeleton can effectively prevent the further expansion of the wear depth of the composite material. The reinforced W skeleton can effectively prevent deep
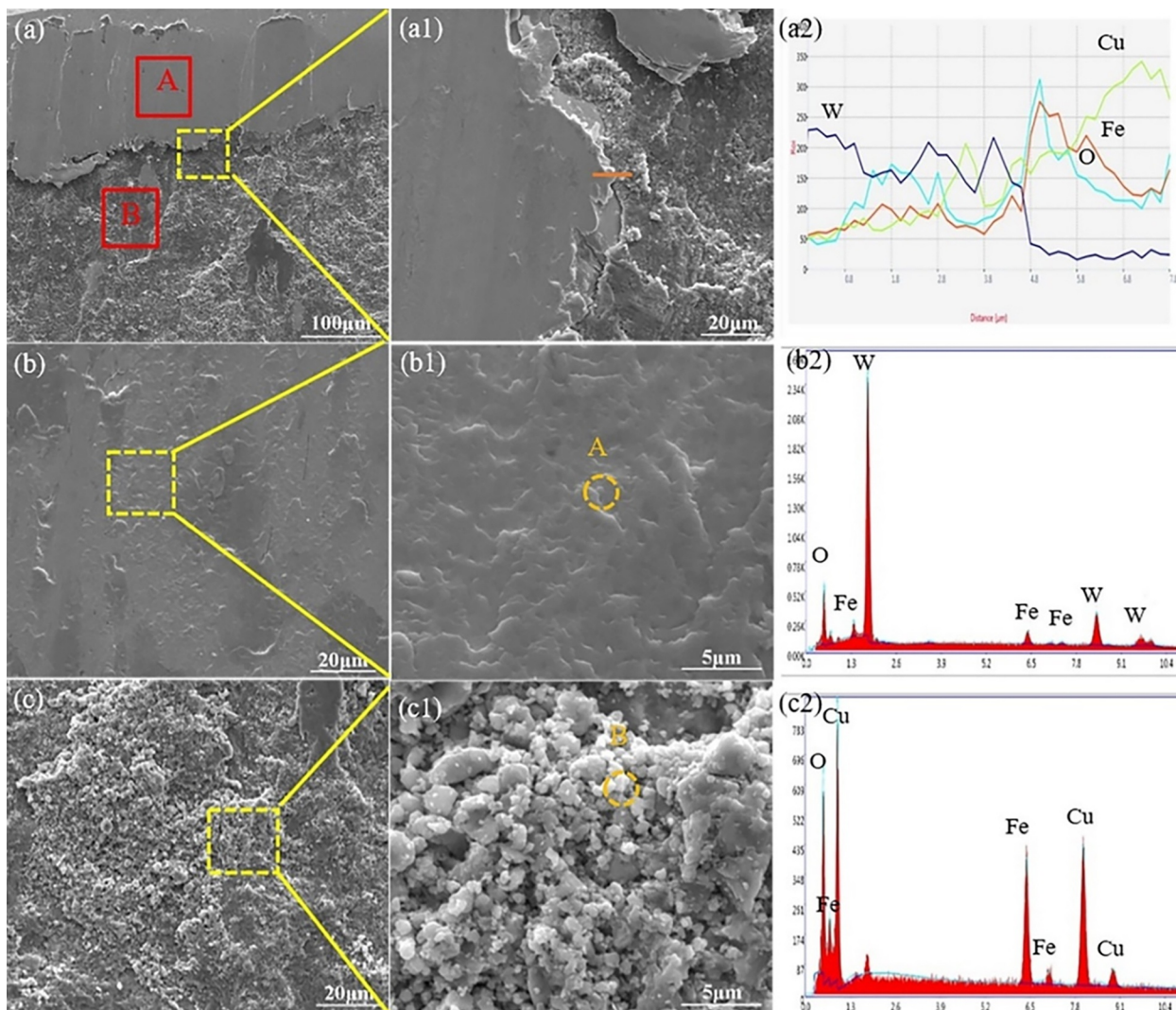
Figure 11. Surface morphologies of copper tungsten composites worn at 300℃ (a1-a2) The magnified part of the composite material after wear and its EDS spectrum; (b-b1) The enlarged part of region a in figure (a) and its EDS spectrum; (c-c1) Enlarged portion of region B in figure (a) and its EDS spectrum.

wear, thus reducing the wear degree of the composite material.

Figure 12 shows the SEM images of Cu-10W composites after friction and wear at 25°C and 300°C. Figure 12(a–c) show the friction and wear morphology at room temperature. It can be seen from Figure 12(a) that there are scratches and furrows in the W and Cu phases which are related to friction and wear at 25°C. Compared with the friction and wear scratches and trenches at 25°C of Cu-30W composites, the typical abrasive wear morphology [47] of Cu-10W composites lead to more serious wear loss than Cu-30W composites, which is mainly related to the W content in the composites. This also indicates that the W skeleton has a protective effect on the friction and wear of the composites. As can be seen from the wear morphology at 300°Cshown in Figure 12(d,e,f), scratches and furrow morphology in the material are significantly reduced compared with friction and wear at 25°C, which is mainly related to material's softening effect at the higher temperature. EDS analysis show

that the O element appears in the material, which may be caused by oxidation during friction and wear at the high temperature. The change of O content in Cu phase region is obvious. The severe wear in the Cu phase region is mainly in the form of adhesive wear with apparent Cu phase shedding. However, the wear of W phase is much less significant.

3.3. Arc ablation of composite materials

Figure 13(a~a2) show the SEM images of the surface morphology of tungsten skeleton of Cu-10W composite after the first arc breakdown. There is severe ablation at the surface of tungsten phase but without splash phenomena or breakdown. The erosion area is small. Arc is mainly concentrated in small areas of tungsten skeleton. This is because the tungsten has a high melting point, and the arc process's temperature is not high enough to melt it. Copper droplets appear to form around the ablation center due to the splashing of molten copper from the tungsten
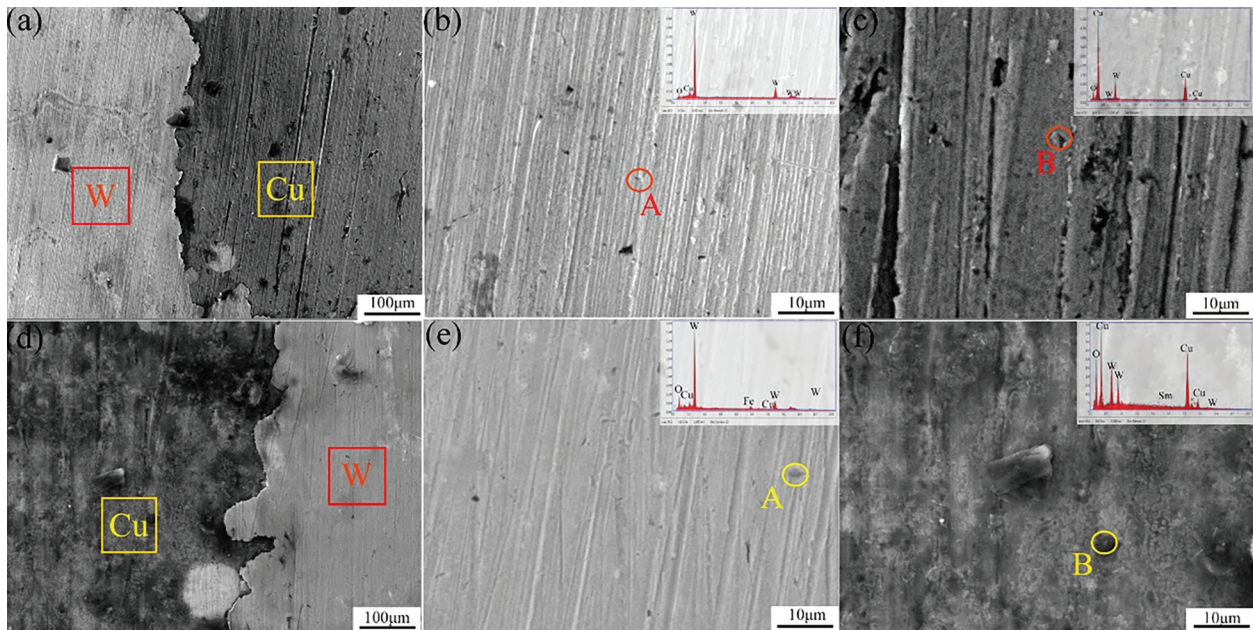
Figure 12. Surface morphologies of copper tungsten composites worn at 25°C and 300°C. (a) The magnified part of the composite material after wear at 25°C; (b) The enlarged part of region a of W in figure (a); (c) Enlarged portion of region B of Cu in figure (a); (d) The magnified part of the composite material after wear at 300°C; (e) The enlarged part of region a of W in figure (d); (f) Enlarged portion of region B of Cu in figure (d).
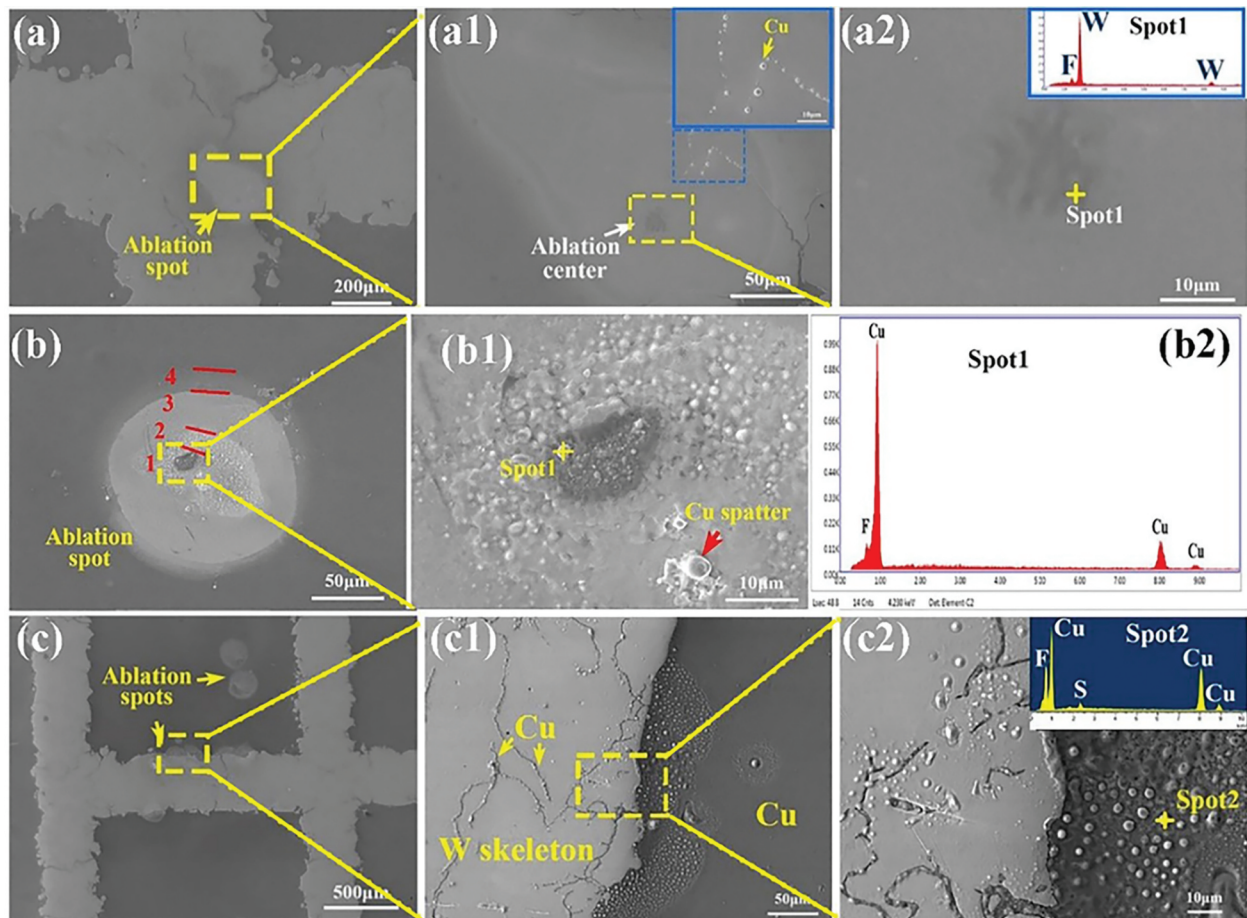
Figure 13. SEM of network-shaped tungsten reinforced copper matrix composites after the first breakdown; (a-a2) The surface morphology and EDS spectrum of the exact breakdown on tungsten skeleton; (b-b2) The surface morphology and EDS spectrum of the exact breakdown on pure copper phase; (c-c2) The surface morphology and EDS spectrum of the exact breakdown on the interface of composite materials.

skeleton. Figure 13(b~b2) show the microstructures of the initial breakdown. At the breakdown point, the ablation products are still attached to the surface. The breakdown area is circular and can be divided into four regions from inside to outside, i.e. the severely ablative central zone, the molten zone of copper liquid, the strong heat affected zone and the weak heat affected zone. Figure 13(c~c2) show the morphologies of arc head breakdown at the Cu/W interface. There are multiple ablation centers, which exist not only in the composite interfaces, but also in the pure copper phase. The shape of the ablation pit is circle, and the ablation pit at the interface tends to develop along the ablation interface. The copper is splashed onto the surface to form a clear pattern due to its low melting point. Some cracks can be observed due to the electric breakdown. EDS analysis of rough protrusions in the copper phase shows that all of them are formed during splashing at the high temperature.

Figure 14 shows the SEM images of Cu-10W composite with a square shape network after 100 times of arc ablation. The breakdown position is always at the copper-tungsten interface. Figure 14(a) shows that the severe ablations process is concentrated in the pure copper phase. The red dotted line in this figure shows that the severe ablations often occur at tungsten skeletons adjacent to the breakdown point. For the pure copper, there are normally four layers of ablation halos generated when the copper is broken down. Whereas the outer halo of square shaped network Cu-10W composite is not obvious after several times of ablation. The main reason for this difference is that the pure copper has a low work function, thus in the first breakdown, tungsten is difficult to strike through. The morphologies of copper and tungsten after 100 times of ablation are dramatically different. The tungsten

skeleton appears to have an enhancement effect of the ablation resistance for the composites. The Cu/W interfaces at the breakdown center show that severe ablations occurred in the Cu phase while no obvious ablations were observed in the tungsten skeleton. EDS analysis show that the copper phase is dominant with a small amount of S and F elements in tungsten phase. There is also an obvious cracking phenomenon in the copper phase, which is mainly caused by effect of SF_6 in the chamber. The CuF_2 is formed between elements of F and Cu during the multiple ablations [48], which is attached to the pure copper phase. The tungsten phases are remained intact with only some bumps appeared on the surface. EDS analysis of these bumps show that tungsten is the main element with a small amount of copper contents. The copper element is mainly caused by the splashing of copper phase during breakdown. The network-like tungsten phase prepared by 3D printing prevents the spillage and spatter of copper phase in the ablation process, so the surface of the composite remains intact after hundreds of ablations.

Figure 15 shows the arc ablation mechanism of CuW composites. Arc ablation of CuW composites can be divided into two stages. During the initial arc breakdown, the ablation area is mainly dominated by the melting evaporation of Cu phase [48]. At this stage, the arc releases the breakdown electrons and bombards the composite material, causing the Cu atoms on the surface to overflow the surface. They are then melt and evaporated under the action of high temperature. This is because the work function of the Cu phase is lower than that of the W phase (φCu(4.36 eV) & φW(4.55 eV) [49], and the melting point of copper phase is low [48]. The melting evaporation of Cu phase takes away a lot of heat [50], which plays a cooling role for the
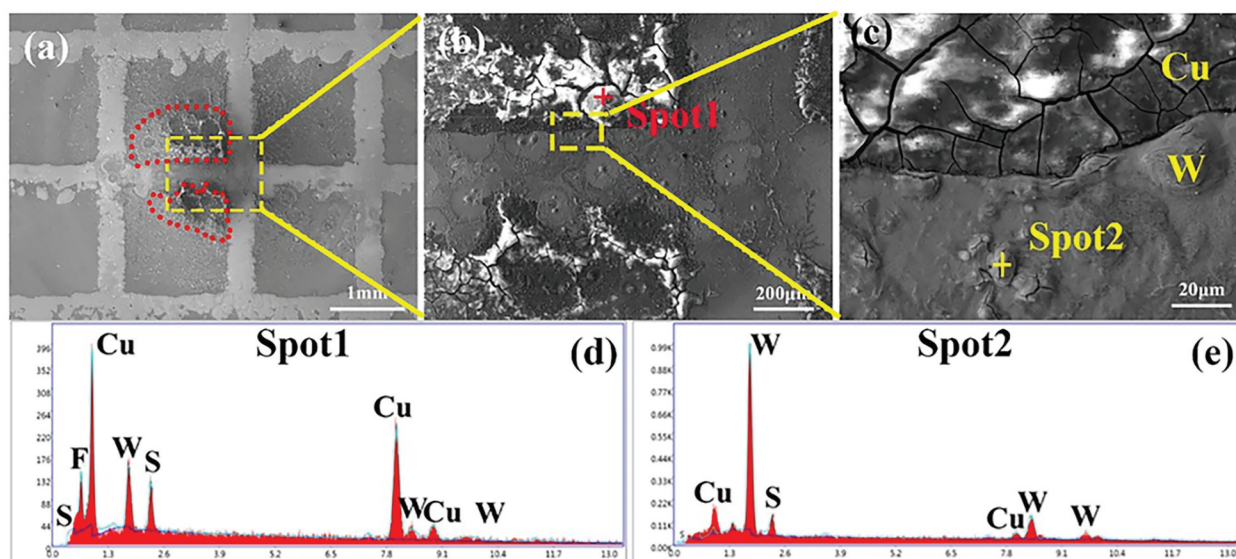
Figure 14. SEM images of 100 times ablation of Cu-10W composite prepared by Cu-phase square melting in tungsten framework; (a) Macroscopic feature; (b) Breakdown center; (c) Micro-area magnification of (b); (d) EDS of spot 1; (e) EDS of spot 2.
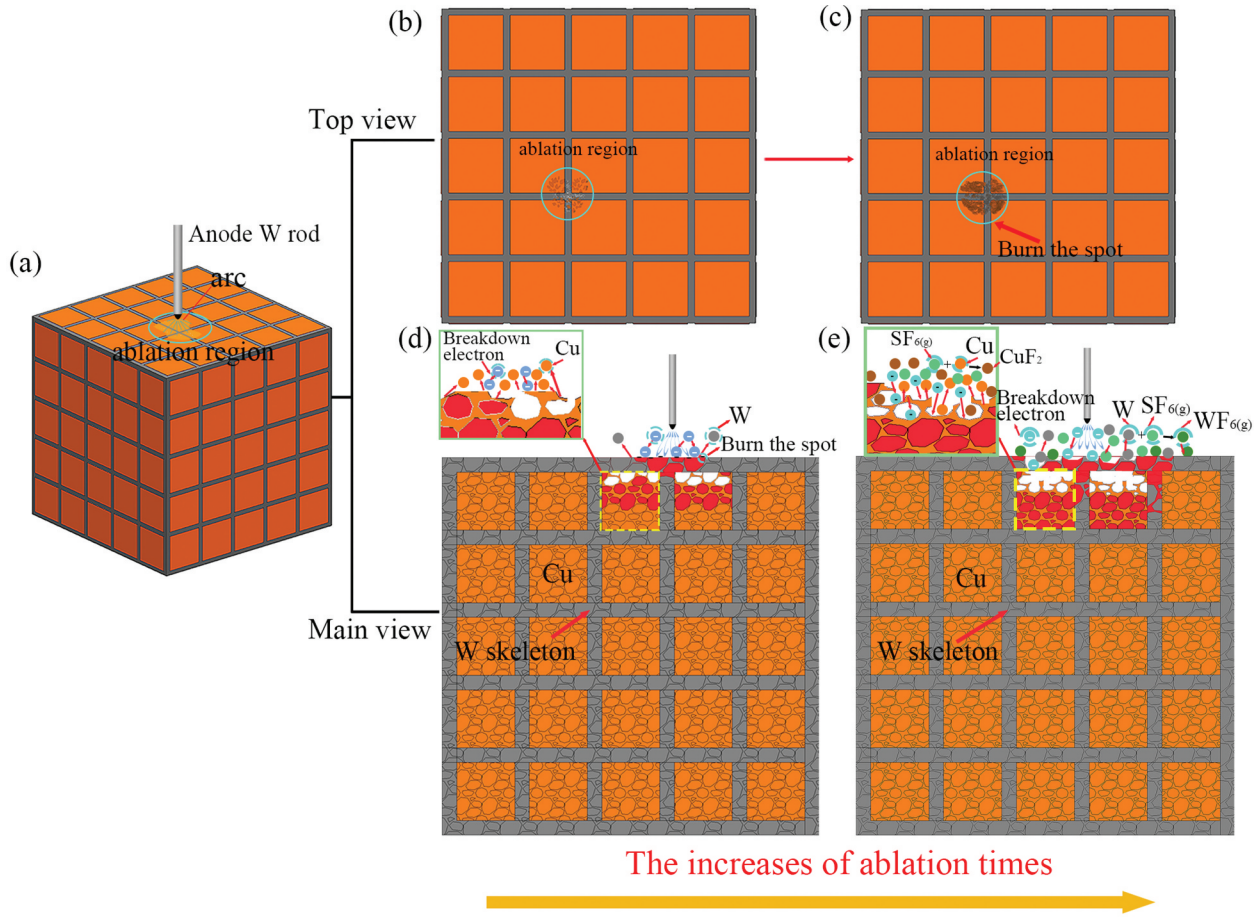
Figure 15. Schematic representation of CuW composites arc breakdown: (a) Macroscopic in ablation; (b,c) Burn spot under different breakdown times; (d,e) The change of ablative structure under different breakdown times.

W skeleton and improves the ablative resistance of W skeleton. As a result, there are obvious ablative marks of Cu phase in the ablative area, while there are only a few ablative spots on the W skeleton.

With the increase of arc breakdown times, more and more particles are broken down and spilled in composite materials, and the ablation area is increasing. Obvious ablation pits and ablation spots are gradually formed in the ablation area, which are formed when the W and Cu atoms are gradually melted and evaporated from the material surface and produce mutual sputtering under the bombardment of breakdown electrons. At the same time, SF6 gas is ionized and reacts with the spilled Cu and W on the surface of the composite material to generate CuF_2 particles and WF_6 gas (the reaction equations are shown in Equations (3–5)) [48], and then volatilizes to the surface of the composite material by sputtering [51].

$$3SF_6 + W \rightarrow WF_6(g) + 3SF_4 \qquad (3)$$

$$SF_6 + Cu \rightarrow CuF_2(s) + SF_4 \qquad (4)$$

$$4SF_6 + 3W + Cu \rightarrow 2S_2F_2(g) + 3WF_6(g) + CuF_2(s) \quad (5)$$
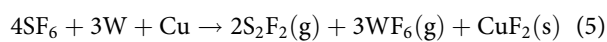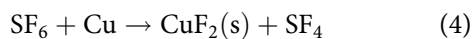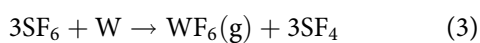
On the one hand, the existence of W skeleton hinders the spreading of Cu phase melting evaporation. On the other hand, its low ablation enables the composite to maintain a complete structure after the ablation. The melting evaporation of Cu phase takes away a lot of heat, which also plays a cooling effect on W skeleton and alleviates the overall ablation of the composite material. Compared with the traditional CuW composites with more W and less Cu, the W skeleton reinforced Cu matrix composites in this study exhibit the interaction of W and Cu phases, which slows down the ablation rate and improves the ablative resistance of the composites.

4. Conclusion

In this paper, tungsten reinforced copper matrix composites with two types of W skeletons were prepared using a SLM technique, in which copper was melted and infiltrated into the tungsten network matrix. Results showed that the electrical conductivity, thermal conductivity, and mechanical properties of the composites were greatly affected by the content of two components (W and Cu). Among them, the composite with 90% Cu content has shown the highest conductivity, 80.3% IACS, and the highest thermal conductivity (375.4 W/(m·K), 25°C). The tensile strength is 135

MPa, and the tensile fracture shows folded morphology, mainly the ductile fracture. At the same time, in order to explore the influence of W skeleton, the impact toughness and friction and wear properties of Cu-30W and Cu-10W composites were studied. The results show that the impact toughness of Cu-30W and Cu-10W composites are 11.25 and 15.2 J/cm^2. There are two fracture modes observed, i.e. cleavage brittle fracture and ductile fracture. The friction coefficients at 25°C and 300°C are ∼ 0.8 and ∼ 0.45. The wear rates after 70 min are 0.367 mg and 2.83 mg.

The arc ablation tests show that the first breakdown of the composites occurs in the copper phase, resulting in circular ablative points surrounded by ablative products. In the tungsten network phase, the breakdown pit is shallow, and the erosion area is small. The arc is mainly concentrated in a small area of tungsten skeleton. When the first breakdown happens at the interface, the ablation pit tends to develop along the ablation interface, and the molten copper in the skeleton is splashed onto the surface. After several arc breakdowns, the ablation pits of the tungsten reinforced copper matrix composites are quite small and the tungsten skeleton elements remain intact. This shows the good performance of the composites in the arc ablation.

Disclosure statement

No potential conflict of interest was reported by the author(s).

Data availability statement

All data generated or analyzed during this study are included in this published article (and its supplementary information files).

References

[1] Tazegul O, Dylmishi V, Cimenoglu H. Copper matrix composite coatings produced by cold spraying process for electrical applications. Arch Civil Mech Eng. 2016;16(3):344–350. doi: 10.1016/j.acme.2016.01.005

[2] Guo X, Jia L, LÜ Z, et al. Research status and development trend of particle reinforced copper matrix composites. Mater Mech Eng. 2023;47(5):109–117.

[3] Sathiskumar R, Murugan N, Dinaharan I, et al. Characterization of boron carbide particulate reinforced in situ copper surface composites synthesized using friction stir processing. Mater Charact. 2013;84:16–27. doi: 10.1016/j.matchar.2013.07.001

[4] Akbarpour MR, Farvizi M, Kim HS. Microstructural and kinetic investigation on the suppression of grain growth in nanocrystalline copper by the dispersion of silicon carbide nanoparticles. Mater Design. 2017;119:311–318. doi: 10.1016/j.matdes.2017.01.077

[5] Qin YQ, Tian Y, Peng YQ, et al. Research status and development trend of preparation technology of ceramic particle dispersion strengthened copper-matrix composites. J Alloys Compd. 2020;848:156475. doi: 10.1016/j.jallcom.2020.156475

[6] Wang L, Zheng C, Kombaiah B, et al. Contrasting roles of Laves_Cr2Nb precipitates on the creep properties of novel CuCrNbZr alloys. Mater Sci Eng A. 2020;779:139110. doi: 10.1016/j.msea.2020.139110

[7] Yu C, Xiaohong Y, Xuejian L, et al. Effects of addition model and content of Zr on microstructure and properties of CuCrZr alloy. Hot Working Technol. 2017;46(15):90–93+97. doi: 10.14158/j.cnki.1001-3814.2017.15.021

[8] Guohui L, Sixiang Z, Lingjian P, et al. Control of precipitates in CuCrZr alloy. Heat Treat Met. 2015;40(4):1–6. doi: 10.13251/j.issn.0254-6051.2015.04.001

[9] Guo C, Zhan Z, Quan L. Study of the preparation and properties of 0.5 vol% Ni-CNTs/Cu nanocomposites with magnetic alignment. J Alloys Compd. 2019;781:261–269. doi: 10.1016/j.jallcom.2018.12.028

[10] Kim KT, Cha SI, Hong SH. Hardness and wear resistance of carbon nanotube reinforced Cu matrix nanocomposites. Mater Sci Eng. 2007;449–451:46–50. doi: 10.1016/j.msea.2006.02.310

[11] Sano N, Naito M, Kikuchi T. Enhanced field emission properties of films consisting of Fe-core carbon nanotubes prepared under magnetic field. Carbon. 2007;45(1):78–82. doi: 10.1016/j.carbon.2006.08.003

[12] Bai S, Guan L, Zhang Y, et al. Enhanced tribological, electrical, and thermal properties of SiC/Cu composites by SiO2–Cu2O glass phase modification. Ceram Int. 2023;50:750–756. doi: 10.1016/j.ceramint.2023.10.153

[13] Feng J, Song K, Liang S, et al. Mechanical properties and electrical conductivity of oriented-SiC-whisker-reinforced Al2O3/Cu composites. J Mater Res Technol. 2022;20:1470–1480. doi: 10.1016/j.jmrt.2022.07.131

[14] Li X, Zhang M, Zhang G, et al. Effect of spark plasma sintering temperature on structure and performance characteristics of Cu-20wt%W composite. J Alloys Compd. 2022;912:165246. doi: 10.1016/j.jallcom.2022.165246

[15] Li R, Chen W, Zhou K, et al. Freeze-casted tungsten skeleton reinforced copper matrix composites. J Alloys Compd. 2023;960:170859. doi: 10.1016/j.jallcom.2023.170859

[16] Zhao Z, Tang F, Hou C, et al. Uncover the mystery of interfacial interactions in immiscible composites by

spectroscopic microscopy: a case study with W-Cu. J Mater Sci Technol. 2022;126:106–115. doi: 10.1016/j.jmst.2022.03.014

[17] Wang X, Wei S, Xu L, et al. Effect of sintering temperature on fine-grained CuW composites with high copper. Mater Charact. 2019;153:121–127. doi: 10.1016/j.matchar.2019.04.017

[18] Leema N, Radha P, Vettivel SC, et al. Characterization, pore size measurement and wear model of a sintered Cu–W nano composite using radial basis functional neural network. Mater Design. 2015;68:195–206. doi: 10.1016/j.matdes.2014.11.035

[19] Shi Y, Chen W, Dong L, et al. Enhancing copper infiltration into alumina using spark plasma sintering to achieve high performance Al2O3/Cu composites. Ceram Int. 2018;44(1):57–64. doi: 10.1016/j.ceramint.2017.09.062

[20] Cooke S, Ahmadi K, Willerth S, et al. Metal additive manufacturing: technology, metallurgy and modelling. J Manuf Processes. 2020;57:978–1003. doi: 10.1016/j.jmapro.2020.07.025

[21] Thijs L, Montero Sistiaga ML, Wauthle R, et al. Strong morphological and crystallographic texture and resulting yield strength anisotropy in selective laser melted tantalum. Acta Materialia. 2013;61(12):4657–4668. doi: 10.1016/j.actamat.2013.04.036

[22] Ambruş S, Muntean R, Codrean C, et al. Influence of printing conditions on the mechanical properties of copper-polylactic acid composites obtained by 3D printing fused deposition modelling. Mater Today Proc. 2023;72:580–585. doi: 10.1016/j.matpr.2022.10.061

[23] Dai D, Gu D. Thermal behavior and densification mechanism during selective laser melting of copper matrix composites: simulation and experiments. Mater Design. 2014;55:482–491. doi: 10.1016/j.matdes.2013.10.006

[24] Li R, Chen W, Zhou K, et al. Deformation and fracture mechanisms of selective laser melted tungsten skeleton reinforced copper matrix composites at varied temperatures. Mater Lett. 2023;332:133550. doi: 10.1016/j.matlet.2022.133550

[25] Zhou K, Chen W, Yang Y, et al. Microstructure and mechanical behavior of porous tungsten skeletons synthesized by selected laser melting. Int J Refract Metals Hard Mater. 2022;103:105769. doi: 10.1016/j.ijrmhm.2021.105769

[26] Tan C, Zhou K, Ma W, et al. Selective laser melting of high-performance pure tungsten: parameter design, densification behavior and mechanical properties. Sci Technol Adv Mater. 2018;19(1):370–380. doi: 10.1080/14686996.2018.1455154

[27] Zhao Y, Jiancheng T, Ye N, et al. Microstructure and properties of WC@W-Cu composites prepared by composite electroplating. Rare Metal Mater Eng. 2021;50(4):1384–1390.

[28] Zhu S, Fan JL, Liu T, et al. Electric conductivities of ultrafine W-Cu materials. Zhongguo Youse Jinshu Xuebao/Chin J Nonferrous Met. 2010;20:1360–1364.

[29] Yu Y, Zhang W, Yu H. Effect of Cu content and heat treatment on the properties and microstructure of W–Cu composites produced by hot extrusion with steel cup. Adv Powder Technol. 2015;26(4):1047–1052. doi: 10.1016/j.apt.2015.04.012

[30] Wang J, Li JJ, Weng GJ, et al. The effects of temperature and alignment state of nanofillers on the thermal conductivity of both metal and nonmetal based

graphene nanocomposites. Acta Materialia. 2020;185:461–473. doi: 10.1016/j.actamat.2019.12.032

[31] Li J, Wenge C, Wenjun T, et al. Study on W fiber reinforced W-Cu composites with high Cu content. Powder Metall Technol. 2012;30(2):125–129. doi: 10.3969/j.issn.1001-3784.2012.02.008

[32] Prokhorov V, Bagramov R, Gerasimov V, et al. Copper and its alloys thermal conductivity controlling with diamond and Ti or Cr addition. Mater Today Proc. 2018;5(12):26104–26107. doi: 10.1016/j.matpr.2018.08.037

[33] Varol T, Güler O, Akçay SB, et al. Enhancement of electrical and thermal conductivity of low-cost novel Cu–Ag alloys prepared by hot-pressing and electroless plating from recycled electrolytic copper powders. Mater Chem Phys. 2022;281:125892. doi: 10.1016/j.matchemphys.2022.125892

[34] Duan J, Guo X, Huang T, et al. Arc ablation resistance behavior of Cu-W alloys with different W contents under atmospheric environment. Mater Today Commun. 2023;34:105173. doi: 10.1016/j.mtcomm.2022.105173

[35] Lu T, Chen C, Li P, et al. Enhanced mechanical and electrical properties of in situ synthesized nano-tungsten dispersion-strengthened copper alloy. Mater Sci Eng A. 2021;799:140161. doi: 10.1016/j.msea.2020.140161

[36] Lu T-X, Chen C-G, Guo Z-M, et al. Tungsten nanoparticle-strengthened copper composite prepared by a sol-gel method and in-situ reaction. Int J Miner Metall Mater. 2019;26(11):1477–1483. doi: 10.1007/s12613-019-1889-3

[37] Li SJ, Xu QS, Wang Z, et al. Influence of cell shape on mechanical properties of Ti-6Al-4V meshes fabricated by electron beam melting method. Acta Biomater. 2014;10(10):4537–4547. doi: 10.1016/j.actbio.2014.06.010

[38] Zhang C, Zhu H, Hu Z, et al. A comparative study on single-laser and multi-laser selective laser melting AlSi10Mg: defects, microstructure and mechanical properties. Mater Sci Eng A. 2019;746:416–423. doi: 10.1016/j.msea.2019.01.024

[39] Cui Q. Preparation and properties of graphite/copper composites with high thermal conductivity. Beijing: University of Science and Technology Beijing; 2021.

[40] Li X, Yan F, Zhang F, et al. Effect of TipSnC mass fraction on microstructure and properties of copper matrix composites. Chin Foundry Equip Technol. 2020;55(1):12–18.

[41] Gao H. Effect of heat treatment on hardness and lmpact toughness of polynary copper alloy. Phys Examination Test. 2007;145:17–19. doi: 10.13228/j.boyuan.issn1001-0777.2007.01.005.

[42] Huang Y, Zhou X, Hua N, et al. High temperature friction and wear behavior of tungsten – copper alloys. Int J Refract Metals Hard Mater. 2018;77:105–112. doi: 10.1016/j.ijrmhm.2018.08.001

[43] Ravi M, Ranocchiari M, Van bokhoven JA. The direct catalytic oxidation of methane to methanol—a critical assessment. Angew Chem Int Ed. 2017;56(52):16464–16483. doi: 10.1002/anie.201702550

[44] Xiao Y, Cheng Y, Shen M, et al. Friction and wear behavior of copper metal matrix composites at temperatures up to 800°C. J Mater Res Technol. 2022;19:2050–2062. doi: 10.1016/j.jmrt.2022.05.192

[45] Park CW, Shin MW, Jang H. Friction-induced stick-slip intensified by corrosion of gray iron brake

disc. Wear. 2014;309(1–2):89–95. doi: 10.1016/j.wear.2013.11.008

[46] Zhimeng T, Zemin W, Lei X, et al. Thermal and tribological properties of MoS2 doped graphite/copper composites by microwave sintering. J Mater Res Technol. 2021;15:6001–6010. doi: 10.1016/j.jmrt.2021.11.053

[47] Zhang Q, Yang J, Deng N, et al. Effect of carburized time on microstructure and properties of W Cu composites fabricated by vacuum pulse carburization. Int J Refract Metals Hard Mater. 2023;112:106168. doi: 10.1016/j.ijrmhm.2023.106168

[48] Zhou YX, Xue YL, Zhou K. Failure analysis of arc ablated tungsten-copper electrical contacts. Vacuum. 2019;164:390–395. doi: 10.1016/j.vacuum.2019.03.052

[49] Chen W, Xing L, Li J. Unusual arc distribution on surface and electrical breakdown mechanism of nanocrystalline tungsten copper alloy. Xiyou Jinshu Cailiao Yu Gongcheng/Rare Metal Mater Eng. 2007;36:463–466.

[50] Ma D, Xie J, Li J, et al. Contact resistance and arc erosion of tungsten-copper contacts in direct currents. J Wuhan Univ Technol-Mater Sci Ed. 2017;32(4):816–822. doi: 10.1007/s11595-017-1674-y

[51] Chen W, Shi Y, Dong L, et al. Infiltration sintering of WCu alloys from copper-coated tungsten composite powders for superior mechanical properties and arc-ablation resistance. J Alloys Compd. 2017;728:196–205. doi: 10.1016/j.jallcom.2017.08.164